
Article:
Stefanou, G orcid.org/0000-0002-8017-9498, Menges, F, Boehm, B et al. (8 more authors) (2021) Scanning Thermal Microscopy and Ballistic Phonon Transport in Lateral Spin Valves. Physical Review Letters, 127 (3). 035901. ISSN 0031-9007

https://doi.org/10.1103/physrevlett.127.035901

Scanning Thermal Microscopy and Ballistic Phonon Transport in Lateral Spin Valves

G. Stefanou,[1] F. Menges,[2] B. Boehm,[2] K. A. Moran,[1] J. Adams,[1] M. Ali,[1] M. C. Rosamond,[3] B. Gotsmann,[2] R. Allenspach,[2] G. Burnell,[1] and B. J. Hickey[1]

[1] *School of Physics and Astronomy, University of Leeds, LS2 9JT, Leeds, UK.*
[2] *IBM Research - Zurich, Säumerstrasse 4, 8803, Rüschlikon, Switzerland.*
[3] *School of Electronics and Electrical Engineering, University of Leeds, LS2 9JT, Leeds, UK.*

(Dated: July 12, 2021)

Using scanning thermal microscopy we have mapped the spatial distribution of temperatures in an operating nanoscale device formed from a magnetic injector, a Ag connecting wire, and a magnetic detector. An analytical model explained the thermal diffusion over the measured temperature range (2 K – 300 K) and injector-detector separation (400 nm – 3000 nm). The characteristic diffusion lengths of the Peltier and Joule heat differ remarkably below 60 K, a fact that can be explained by the onset of ballistic phonon heat transfer in the substrate.

The discovery and controversy of the spin-related Seebeck effects [1, 2], the spin-dependent Peltier effect [3, 4] and the spin-dependent magnetothermopower [5–7] *inter alia* have given rise to the field of spin caloritronics [8–10] where the close connection between spin currents and thermal effects are exploited in energy-related devices. More generally, the study of heat transport in nanostructures has highlighted the dimensional effects of many of the transport properties, in particular, the thermal conductivity [11–13] where for nanotubes, it was suggested that at low temperatures phonon transport could be ballistic. There are now several papers demonstrating that the length dependence of the phonon thermal conductivity is a signature of ballistic transport [14, 15]. The wave nature of phonon transport has resulted in the observation of phonon localisation [16] and ballistic phonon waveguides [17]. It is therefore prudent to consider the consequences of potential ballistic phonon transport in the substrates of nanostructures.

Recently, increasing attention has been paid to thermal effects in nanostructures known as lateral spin valves (LSVs), notably: electrical v. thermal spin injection and calculations of the thermal gradients [1, 18–20], the temperature dependence of spin transport [21], Joule heating and the anomalous Nernst-Ettingshausen effect [22, 23], magnetothermal effects on spin relaxation [24] and spin-heat accumulation [25].

LSVs are the archetypal spin current device utilising charge currents which generate heat and since ferromagnets have large Seebeck coefficients (S(T)), *most* of the voltage measured at the detector of a LSV is thermally generated [18]. The non-local resistance (R_s) is conventionally expressed by dividing the detector voltage by the injection current. The field dependence of R_s separates the spin current signal from the thermal signals: R_s is lower for the antiparallel than the parallel configurations of the ferromagnetic (FM) electrodes.

Johnson and Silsbee [26] pointed out that there was an asymmetry in R_s that cannot be due to the spin current. The average non-local resistance of the parallel and antiparallel states (the *baseline resistance* (BLR)) varied with temperature and they proposed it was due to a non-uniform current distribution in the sample, however Bakker *et al* [18] demonstrated that the BLR was primarily due to the Peltier effect. There is an intriguing fact about the BLR that has not been discussed: below 100 K the BLR goes rapidly to near zero where the thermopower of the junction cannot be zero and there is still substantial Joule heating (see Fig. 1(d)). Note that the voltage associated with Joule heating has a low temperature *increase* where the resistance is constant. Other observations of the thermal behaviour need to be understood: Kasai *et al* [27] showed that in LSVs fabricated on substrates with different thermal conductivities, although R_s was the same for both substrates, the magnitude of the BLR was dramatically reduced for the higher thermal conductivity substrate.

The diffusion of Joule and Peltier heat have the same length scale (as they should) as a function of temperature between $\sim$ 60 K and room temperature. But, below 60 K, the Joule heat diffusion length *increases* while the BLR diffusion is no longer exponential and disappears on a short length scale. These observations can only be explained by a more quantitative treatment of the data.

The samples were deposited using the technique of shadow evaporation which relies on the different development rates of resists [28]. They consisted of Permalloy (Py) electrodes connected by Ag wires (100 nm x 100 nm) with a range of electrode separations (400 - 3000 nm). An SEM image of a completed device is shown in Fig. 1(a) with the essential components labelled. Measurements consist of current-voltage characteristics (IV) varying the injector current between $\pm$ 0.5 mA whilst measuring the detector voltage. A quadratic function in the current (I) was fitted to extract the Joule heating term, a linear term which is field dependent (R_s) and a constant related to the voltmeter offset. Fig. 1(b) shows R_s derived from the field dependent linear term as a function of magnetic field. The characteristic shape is due to the magnetic switching of the electrodes that are engineered

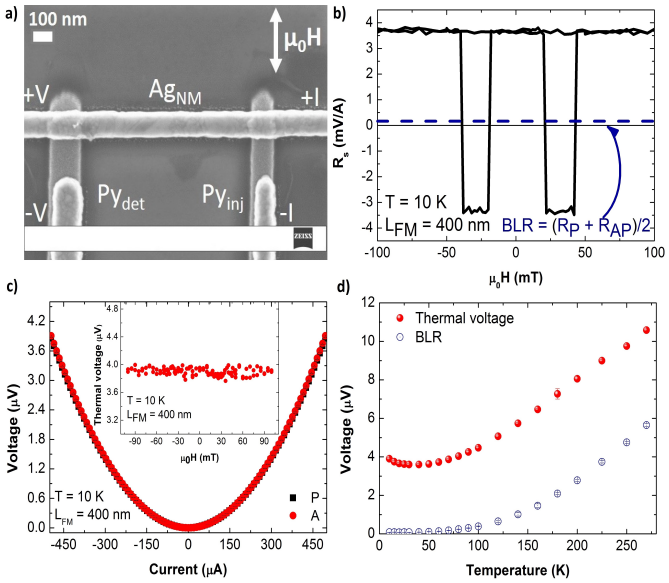

FIG. 1. *(a) A scanning electron microscope (SEM) image of a device. (b) R_s at 10 K for an electrode separation of 400 nm with the BLR. (c) The quadratic term in the fit to the IV measurements showing no difference between the parallel and antiparallel electrode alignment and inset: as a function of magnetic field. (d) Shows the temperature dependence of the Joule heating and the BLR as detector voltages.*

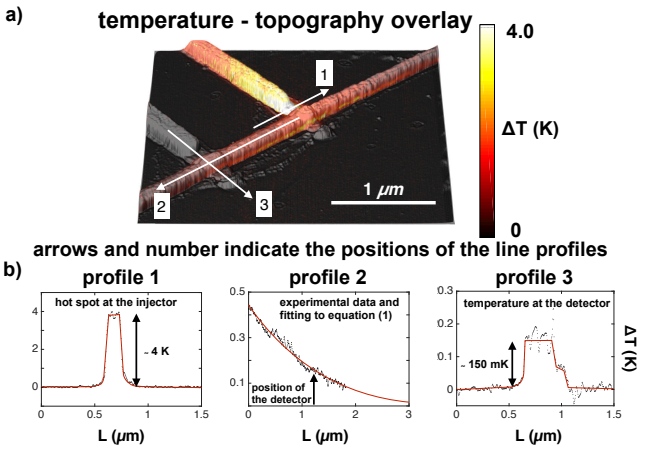

FIG. 2. *(a) SThM image at room temperature showing both topography and temperature rise above the substrate (b) shows the temperature scans across the injector (1), the conduit, including fit (2) and the detector/conduit junction (3).*

to have distinct antiparallel (lower resistance) and parallel (higher resistance) states. The difference between the two states is the spin signal ΔR_s and the average is the BLR.

Fig. 1(c) shows the quadratic term of the IV measurements in the parallel and antiparallel electrode configurations showing that they are the same. The inset shows the quadratic signal as a function of a complete magnetic field sweep. We found that this behaviour was replicated at all temperatures.

We have undertaken thermal imaging on a lateral spin valve *in operando* using Scanning Thermal Microscopy (SThM) [29–32] using an ac current of 1.6 mA passed through the injector. A lock-in amplifier measured the signal from the temperature sensor fabricated into a scanning probe cantilever [29]. The measurements were performed at room temperature in a high vacuum chamber. The method used here [31, 32] can detect independently the two thermal components as the Peltier term is linear in the applied current whereas the Joule heating term has a quadratic dependence and can be detected via the higher harmonic response of the probe.

A small section of the Py electrode is not covered by Ag and indicates a 'hot spot' due to its larger resistance (profile 1 in Fig. 2(b)). The temperature decay along the Ag channel is shown in Fig. 2(a) and is presented as data in (b) profile 2, along with a fit to the data using a model that is described below. Profile 3 shows the temperature distribution across the detector where the rise was about 150 mK. Profiles 1 and 3 extend across the substrate and show that there is negligible temperature rise in the substrate - even very close to the metallic structure. This is useful to inform 3-d finite element models where it can be difficult to estimate the thermal parameters [24, 33].

We have found that a simple analytical model can explain the heat diffusion. We consider a rectangular element of the Ag channel at temperature T with a length dx along the channel, width w and thickness t. The heat diffusing into the cell, $\dot{Q}_{in}$ will equal the sum of the heat that flows through the substrate $\dot{Q}_s$ plus the heat flow that leaves the cell $\dot{Q}_{out}$. The heat flow out of the cell will be: $\dot{Q}_{out} = \dot{Q}_{in} + \frac{d\dot{Q}_{in}}{dx}dx$. For each measurement the system waits for the steady state to establish and therefore T_s, the temperature of the substrate, is a constant at any particular temperature. The heat flow into the substrate will be: $\dot{Q}_s = K(T - T_s)wdx$, where K is the thermal conductance of the interface between Ag and the substrate and wdx is the relevant area for conduction into the substrate. Considering only conduction it is straightforward [28] to show that the equation to solve is:

$$\frac{d^2T'}{dx^2} - \alpha^2 T' = 0 \qquad (1)$$

Where $T' = T - T_s$. The coefficient α^2 is given by:

$$\alpha^2 = \frac{wK}{2\kappa A} = \frac{K}{2\kappa t}$$

where κ is the thermal conductivity of Ag and $A = tw$ is the cross-sectional area of the wire. The factor of 1/2 arises because the diffusion at the injector proceeds in both directions along the Ag wire.

With the boundary conditions that $T(x = 0) = T_{in}$, the temperature of the injector, and $T(x = \infty) = T_s$, the

temperature of the substrate, the solution of this equation is:

$$T(x) = (T_{in} - T_s)e^{-\alpha x} + T_s$$

From the data in Fig. 2 we know the substrate (T_s) and the injector temperatures (T_{in}). Following others [34, 35] we have estimated the thermal conductivity of Ag from the Wiedemann-Franz law and the temperature dependent Lorentz function $\Phi(T)$ [36, 37] which gives us a room temperature value of 240 W/mK which agrees well with other Ag nanowire values [35, 38] leaving only K as a fitting parameter. The best fit (seen in profile 2 of Fig. 2(b)) is in excellent agreement with the data and returns a value of the thermal conductance of 40 ± 2 MW/(m^{2}K) which compares well with the values found for similar metal/dielectric interfaces at room temperature, e.g. Ag on diamond [39] and Au on diamond or sapphire [40]. The length scale of the thermal diffusion is given by $1/\alpha$ and therefore the temperature dependence of the thermal diffusion length is determined by the ratio of the thermal conductivity of Ag to that of the interface conductance.

The veracity of the model has been demonstrated at room temperature but it will apply at any temperature provided the temperature dependence of the thermal parameters is taken into account. We have measured the total thermal voltage and BLR as a function of electrode separation over a range of temperatures. To fit the temperature dependence we used two fitting parameters: the temperature of the injector and the thermal conductance of the Ag/SiO_2 interface, K. Measured detector voltages were converted to temperatures using the published values of the thermopower of Ag [41] and Py [42] nanowires combined into an effective Seebeck coefficient. We extrapolated estimates to low temperatures where data were not available. However, as the temperature of the injector was a fitting parameter, this provided a check that the estimated temperatures were reasonable, and if not, a new estimate of the Seebeck coefficient was determined and the process repeated until consistent.

Example fits to the Joule heating are shown in Fig. 3(a - d) where it can be seen that the data are accounted for remarkably well by the model [28]. In panels (e-h) the BLR data has been fitted where it is evident that below 60 K the model does not fit - the diffusion is no longer exponential.

Fig. 3(i) shows the thermal conductivity of Ag derived from L(T) which agrees well with measured values [35, 38]. The temperature dependence of the interface conductance (K), Fig. 3(j), agrees very well with that directly measured for interfaces such as Al/Si [39], Au on diamond [40] and Al on amorphous SiO_x [43] - both in magnitude and trend with temperature. Fig. 3(k) displays the diffusion length associated with the thermally generated voltages measured at the detector. It is expected that there is only one length scale associated with the diffusion of heat and that is true for temperatures between $\sim$ 60 K to room temperature. The pronounced difference between the Joule and BLR measurements indicates that they are the result of different combinations of thermal effects. The temperature increase of the injector and detector above that of the substrate as a function of temperature is shown in Fig. 3 (l). When the temperature is lowered to about 100 K, both temperatures begin to increase which coincides with the first point of change in the length scales of Fig. 3 (k). This behaviour is determined by the fact that at $\sim$ 100 K the value of the thermal interface conductance diminishes more rapidly when lowering the temperature (see panel (j)). The upshot is that less heat is transferred to the substrate as the temperature is lowered. Since the thermal diffusion length is determined by the ratio of this conductance and the thermal conductivity of Ag, that explains the rise in the Joule diffusion length that starts at $\sim$ 100 K. From 1 (d) it is clear that the BLR voltage is nearly zero below 100 K whereas the Joule voltage is still about 4 μV thus there is no discernible Joule contribution to the BLR. At 100 K, for our samples, the Peltier power is $\sim$ 1 μW and falling rapidly compared to $\sim$ 135 μW from the Joule heating reaching a constant of 120 μW at low temperatures. The Peltier effect happens only at the Py/Ag interface which is not thermally well connected to the substrate and has a comparatively small area. The Joule heat is generated everywhere along the charge current path in metal that is well connected to the substrate and has a very large area. Thus changes in the interface conductance affect the BLR much more than the Joule heating. The simplest explanation for the behaviour of the BLR below 70 K is that the Peltier heat loss to the substrate has all but vanished. That means that the solution to equation 1 becomes $T(x) = \left(\frac{T_s - T_i}{L}\right) x + T_i$, where L is the distance from the injector where $T = T_s$. Although the data is too sparse to test this properly, the data indicates that the linear decrease looks plausible. The observation by Kasai *et al* [27] where the BLR at room temperature was smaller when the thermal conductivity of the substrate was higher, cannot be understood in terms of the Peltier effect. However, it can be seen as a consequence of the thermal interface conductance which is, in part, determined by the thermal conductivity of the substrate.

Interestingly, to fit the low temperature behaviour of either the Joule or BLR data, the heat transfer to the substrate has to be *less* than that accounted for by the thermal conductivity of the substrate i.e. the data cannot be fitted unless the thermal interface conductance is lower than that expected from an interface of sheet film on a substrate. This suggests that the dimensions of the wire become important at low temperatures. At $\sim$ 15 K, the electronic mean free path (mfp) saturates near 100 nm [28] which is the thickness of the Ag wire, therefore transport in the Ag never reaches the quasi-ballistic regime. However the mfp of phonons in the substrate reaches 49 nm at 10 K [44] but this could be an

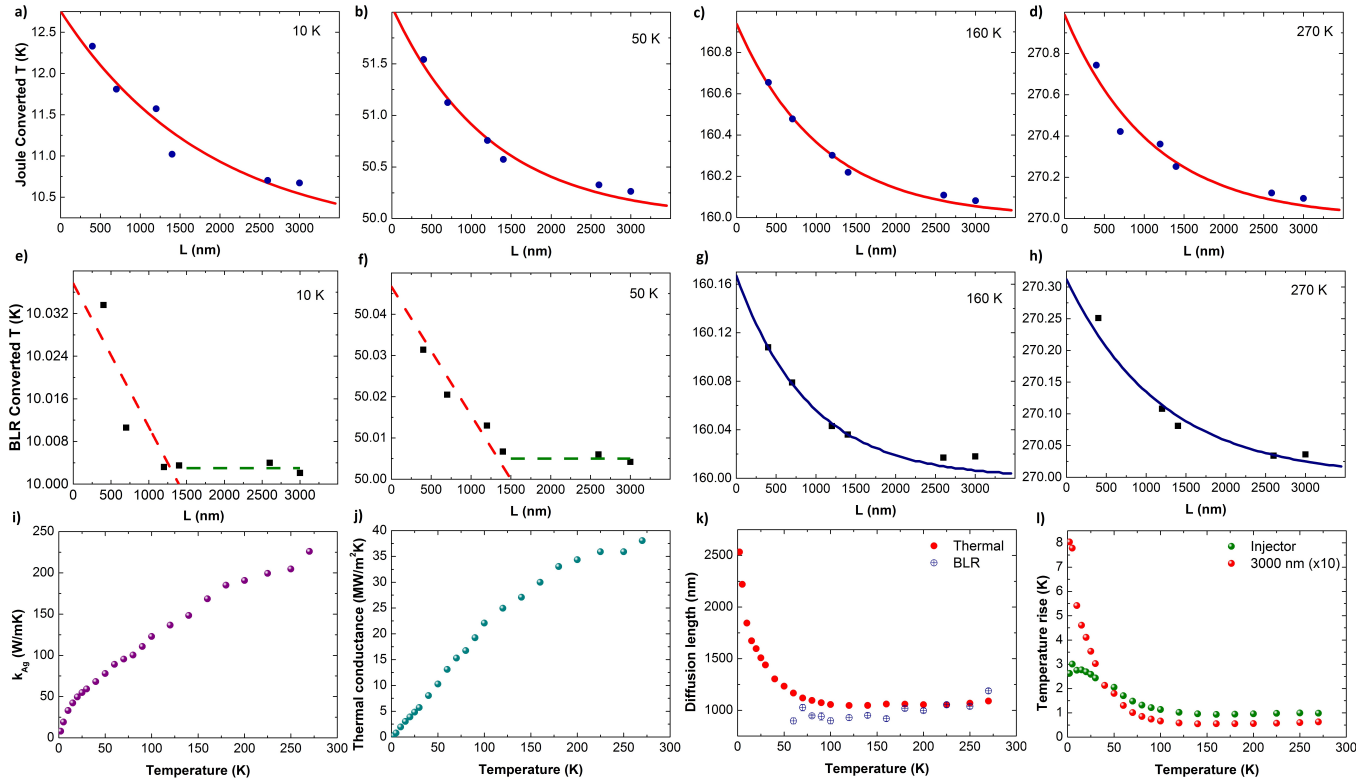

FIG. 3. *Panels (a) to (d) show the exponential decay of Joule heating whereas panels (e) to (h) show the behaviour of the BLR - (e) and (f) show that the diffusion below 50 K is no longer exponential due to the diminishing heat loss to the substrate. Panel (i) is the thermal conductivity of Ag derived from $\Phi(T)$ and agrees well with measured values [35, 38]; (j) is the extracted values of K, the interface conductance; (k) the diffusion length scales associated with the Joule heating and the BLR voltages measured at the detector; (l) shows the temperature rise of the injector and detector for a separation of 3000 nm.*

underestimate by a factor of 10 [45] as it uses the kinetic expression which would account for the fact that we observe the onset of this regime near 50 K. Hence the phonon mfp reaches the width (100 nm) of the Ag wire and therefore we are entering the regime of ballistic heat transfer into the substrate. This is reflected in a large reduction of the interface thermal conductance. We can estimate the lower limit of ballistic conductance from the kinetic expression [46] $K = C\nu = 3\kappa/\Lambda$ where Λ is the phonon mfp, C is the phonon heat capacity and ν is the averaged sound velocity. This gives a value of 0.81 $\mathrm{MWm^{-2}K^{-1}}$ for the interface conductance cf 0.57 $\mathrm{MWm^{-2}K^{-1}}$ returned by the fit at 5 K.

The paradoxical low temperature upturn in the Joule heating voltage (Fig. 1 (d)) is also due to the reduction in the interface thermal conductance due to ballistic transport to the substrate. Despite the low value of the Ag thermal conductivity the ballistic transport to the substrate ensures that more heat is reaching the detector than at slightly higher temperatures.

Using scanning thermal microscopy we have mapped the spatial distribution of temperatures in an operating lateral spin valve. Unexpectedly, the characteristic diffusion lengths for the Joule heating and BLR are remarkably different below 60 K: the Joule diffusion length increases whereas the BLR diffusion decreases and is *not exponential*. The apparent increase in Joule heating where the resistance is constant, is a result of increased het flow to the detector. These surprising results are explained by the analytical model and the fact that at low temperatures the phonon mean free path in the substrate reaches the dimensions of the wire and thus ballistic thermal transport accounts for the apparently anomalous low temperature behaviour of the baseline resistance and Joule heating in lateral spin valves. The model and techniques developed in this paper and the results on phonon coupling are broadly applicable to nanoscale structures on similar substrates.

The authors would like to acknowledge financial support from the European Union Seventh Framework Programme [FP7-People-2012-ITN] under grant agreement 316657 (SpinIcur), the UK funding council EPSRC (EP/M000923) and Leeds alumnus donor P. Mans. We would like to thank C.H. Marrows, J. Barker and D. Greig for fruitful discussions and also A. Bischof, J. Turton, B. Gibbs, L.D.R. Bone, R. Oliver and T. Haynes for their technical expertise. The data associated with this paper is available from University of Leeds at

https://doi.org/10.5518/976.

[1] A. Slachter, F. L. Bakker, J.-p. Adam, and B. J. van Wees, Thermally driven spin injection from a ferromagnet into a non-magnetic metal, Nature Physics **6**, 879 (2010).

[2] M. Schmid, S. Srichandan, D. Meier, T. Kuschel, J.-M. Schmalhorst, M. Vogel, G. Reiss, C. Strunk, and C. H. Back, Transverse spin Seebeck effect versus anomalous and planar Nernst effects in Permalloy thin films, Phys. Rev. Lett. **111**, 187201 (2013).

[3] L. Gravier, S. Serrano-Guisan, F. Reuse, and J.-P. Ansermet, Spin-dependent Peltier effect of perpendicular currents in multilayered nanowires, Phys. Rev. B **73**, 052410 (2006).

[4] J. Flipse, F. L. Bakker, A. Slachter, F. K. Dejene, and B. J. van Wees, Direct observation of the spin-dependent Peltier effect, Nature Nanotechnology **7**, 166 (2012).

[5] E. Avdi, B. J. Hickey, D. Greig, M. A. Howson, M. J. Hall, J. Xu, M. J. Walker, N. Wiser, and P. de Groot, Giant magnetothermopower and giant magnetoresistance in molecular beam epitaxy grown Co/Cu(111) superlattices, Journal of Applied Physics **73**, 5521 (1993).

[6] L. Gravier, F. A. Reuse, A. Rudolf, A. Cachin, J.-E. Wegrowe, and J.-P. Ansermet, Spin-dependent thermopower in Co/Cu multilayer nanowires, Journal of Magnetism and Magnetic Materials **271**, 153 (2004).

[7] Y. Pu, E. Johnston-Halperin, D. Awschalom, and J. Shi, Anisotropic thermopower and planar Nernst effect in $Ga_{1-x}Mn_xAs$ ferromagnetic semiconductors, Phys. Rev. Lett. **97**, 036601 (2006).

[8] G. E. W. Bauer, E. Saitoh, and B. J. van Wees, Spin caloritronics, Nature Materials **11**, 391 (2012).

[9] F. Hellman, A. Hoffmann, Y. Tserkovnyak, G. S. D. Beach, E. E. Fullerton, C. Leighton, A. H. MacDonald, D. C. Ralph, D. A. Arena, H. A. Dürr, P. Fischer, J. Grollier, J. P. Heremans, T. Jungwirth, A. V. Kimel, B. Koopmans, I. N. Krivorotov, S. J. May, A. K. Petford-Long, J. M. Rondinelli, N. Samarth, I. K. Schuller, A. N. Slavin, M. D. Stiles, O. Tchernyshyov, A. Thiaville, and B. L. Zink, Interface-induced phenomena in magnetism, Rev. Mod. Phys. **89**, 025006 (2017).

[10] S. R. Boona, R. C. Myers, and J. P. Heremans, Spin caloritronics, Energy Environ. Sci. **7**, 885 (2014).

[11] P. Kim, L. Shi, A. Majumdar, and P. L. McEuen, Thermal transport measurements of individual multiwalled nanotubes, Phys. Rev. Lett. **87**, 215502 (2001).

[12] T. Meier, F. Menges, P. Nirmalraj, H. Hölscher, H. Riel, and B. Gotsmann, Length-dependent thermal transport along molecular chains, Phys. Rev. Lett. **113**, 060801 (2014).

[13] D. Li, Y. Wu, P. Kim, L. Shi, P. Yang, and A. Majumdar, Thermal conductivity of individual silicon nanowires, Appl. Phys. Lett. **83**, 2934 (2003).

[14] Z. Zhang, Y. Ouyang, Y. Cheng, J. Chen, N. Li, and G. Zhang, Size-dependent phononic thermal transport in low-dimensional nanomaterials, Physics Reports **860**, 1 (2020).

[15] J. Maire, R. Anufriev, and M. Nomura, Ballistic thermal transport in silicon nanowires, Scientific Reports **7**, 41794 (2017).

[16] M. N. Luckyanova, J. Mendoza, H. Lu, B. Song, S. Huang, J. Zhou, M. Li, Y. Dong, H. Zhou, J. Garlow, L. Wu, B. J. Kirby, A. J. Grutter, A. A. Puretzky, Y. Zhu, M. S. Dresselhaus, A. Gossard, and G. Chen, Phonon localization in heat conduction, Science Advances **4** (2018).

[17] A. Tavakoli, K. Lulla, T. Crozes, N. Mingo, E. Collin, and O. Bourgeois, Heat conduction measurements in ballistic 1d phonon waveguides indicate breakdown of the thermal conductance quantization, Nature Communications **9**, 4287 (2018).

[18] F. L. Bakker, A. Slachter, J.-P. Adam, and B. J. van Wees, Interplay of Peltier and Seebeck effects in nanoscale nonlocal spin valves, Phys. Rev. Lett. **105**, 136601 (2010).

[19] F. K. Dejene, J. Flipse, and B. J. van Wees, Spin-dependent Seebeck coefficients of $Ni_{80}Fe_{20}$ and Co in nanopillar spin valves, Phys. Rev. B **86**, 024436 (2012).

[20] A. Hojem, D. Wesenberg, and B. Zink, Thermal spin injection and interface insensitivity in permalloy/aluminum metallic nonlocal spin valves, Phys. Rev. B **94**, 024426 (2016).

[21] A. Pfeiffer, S. Hu, R. M. Reeve, A. Kronenberg, M. Jourdan, T. Kimura, and M. Kläui, Spin currents injected electrically and thermally from highly spin polarized Co_2MnSi, Applied Physics Letters **107**, 082401 (2015).

[22] A. Slachter, F. L. Bakker, and B. J. van Wees, Anomalous Nernst and anisotropic magnetoresistive heating in a lateral spin valve, Phys. Rev. B **84**, 020412 (2011).

[23] S. Hu and T. Kimura, Anomalous Nernst-Ettingshausen effect in nonlocal spin valve measurement under high-bias current injection, Phys. Rev. B **87**, 014424 (2013).

[24] K. Das, F. Dejene, B. van Wees, and I. Vera-Marun, Anisotropic Hanle line shape via magnetothermoelectric phenomena, Phys. Rev. B (R) **94**, 180403 (2016).

[25] F. K. Dejene, J. Flipse, G. E. W. Bauer, and B. J. van Wees, Spin heat accumulation and spin-dependent temperatures in nanopillar spin valves, Nature Physics **9**, 636 (2013).

[26] M. Johnson and R. H. Silsbee, Calculation of nonlocal baseline resistance in a quasi-one-dimensional wire, Phys. Rev. B **76**, 153107 (2007).

[27] S. Kasai, S. Hirayama, Y. K. Takahashi, S. Mitani, K. Hono, H. Adachi, J. Ieda, and S. Maekawa, Thermal engineering of non-local resistance in lateral spin valves, Applied Physics Letters **104**, 162410 (2014).

[28] See Supplementary Information [url] where details of the model, details of the thermal conductivity, Seebeck coefficients and fits to all the data appear including [47, 48] [49–53] [54] [55] [48, 56] [41] [42] [34, 35] [36, 37] [57].

[29] F. Menges, *Scanning Probe Thermometry of Nanosystems*, Ph.D. thesis, ETH (2015).

[30] F. Menges, H. Riel, A. Stemmer, and B. Gotsmann, Quantitative thermometry of nanoscale hot spots, Nano Lett. **12**, 596 (2012).

[31] F. Menges, H. Riel, A. Stemmer, and B. Gotsmann, Nanoscale thermometry by scanning thermal microscopy, Review of Scientific Instruments **87**, 74902 (2016).

[32] F. Menges, P. Mensch, H. Schmid, H. Riel, A. Stemmer, and B. Gotsmann, Temperature mapping of operating nanoscale devices by scanning probe thermometry, Nature Communications **7**, 10874 (2016).

[33] R. K. Bennet, A. Hojem, and B. L. Zink, Thermal gradients and anomalous nernst effects in membrane-

supported nonlocal spin valves, Phys. Rev. B **100**, 104404 (2019).

[34] A. D. Avery, S. J. Mason, D. Bassett, D. Wesenberg, and B. L. Zink, Thermal and electrical conductivity of approximately 100-nm permalloy, Ni, Co, Al, and Cu films and examination of the Wiedemann-Franz law, Phys. Rev. B **92**, 214410 (2015).

[35] D. Kojda, R. Mitdank, M. Handwerg, A. Mogilatenko, M. Albrecht, Z. Wang, J. Ruhhammer, M. Kroener, P. Woias, and S. F. Fischer, Temperature-dependent thermoelectric properties of individual silver nanowires, Phys. Rev. B **91**, 024302 (2015).

[36] R. E. B. Makinson, The thermal conductivity of metals, Math. Proc. Cambridge Philos. Soc. **34**, 474 (1938).

[37] T. M. Tritt, *Thermal Conductivity* (Kluwer, New York, 2004).

[38] J. Wang, Z. Wu, C. Mao, Y. Zhao, J. Yang, and Y. Chen, Effect of electrical contact resistance on measurement of thermal conductivity and Wiedemann-Franz law for individual metallic nanowires, Scientific Reports **8**, 4862 (2018).

[39] C. Monachon, L. Weber, and C. Dames, Thermal Boundary Conductance: A Materials Science Perspective, Annual Review of Materials Research **46**, 433 (2016).

[40] R. J. Stoner and H. J. Maris, Kapitza conductance and heat flow between solids at temperatures from 50 to 300 K, Phys. Rev. B **48**, 16373 (1993).

[41] M. Kockert, D. Kojda, R. Mitdank, A. Mogilatenko, Z. Wang, J. Ruhhammer, M. Kroener, P. Woias, and S. F. Fischer, Nanometrology: Absolute seebeck coefficient of individual silver nanowires, Scientific Reports **9**, 20265 (2019).

[42] A. D. Avery, M. R. Pufall, and B. L. Zink, Determining the planar nernst effect from magnetic-field-dependent thermopower and resistance in nickel and permalloy thin films, Physical Review B **86** (2012).

[43] P. E. Hopkins, Thermal transport across solid interfaces with nanoscale imperfections: Effects of roughness, disorder, dislocations, and bonding on thermal boundary conductance, ISRN Mechanical Engineering **2013**, 682586 (2013).

[44] S.-M. Lee and D. Cahill, Thermal conductivity and specific heat of noncrystalline solids, Phys. Rev. B **4**, 2029 (1971).

[45] M.-H. Bae, Z. Li, Z. Aksamija, P. N. Martin, F. Xiong, Z.-Y. Ong, I. Knezevic, and E. Pop, Ballistic to diffusive crossover of heat flow in graphene ribbons, Nature Communications **4**, 1734 (2013).

[46] M. E. Siemens, Q. Li, R. Yang, K. A. Nelson, E. H. Anderson, M. M. Murnane, and H. C. Kapteyn, Quasi-ballistic thermal transport from nanoscale interfaces observed using ultrafast coherent soft X-ray beams, Nature Materials **9**, 26 (2010).

[47] M. C. Rosamond, J. T. Batley, G. Burnell, B. J. Hickey, and E. H. Linfield, High contrast 3D proximity correction for electron-beam lithography: An enabling technique for the fabrication of suspended masks for complete device fabrication within an UHV environment, Microelectronic Engineering **143**, 5 (2015).

[48] J. T. Batley, M. C. Rosamond, M. Ali, E. H. Linfield, G. Burnell, and B. J. Hickey, Spin relaxation through Kondo scattering in Cu/Py lateral spin valves, Phys.Rev. B **92**, 220420 (2015).

[49] D. Greig, M. Hall, C. Hammond, B. Hickey, H. Ho, M. Howson, M. Walker, N. Wiser, and D. Wright, The giant magnetoresistance of Co/Cu superlattices grown by MBE, Journal Of Magnetism And Magnetic Materials **110**, L239 (1992).

[50] S. M. Poh, X. Zhao, S. J. R. Tan, D. Fu, W. Fei, L. Chu, D. Jiadong, W. Zhou, S. J. Pennycook, A. H. Castro Neto, and K. P. Loh, Molecular Beam Epitaxy of Highly Crystalline $MoSe_2$ on Hexagonal Boron Nitride, ACS Nano **12**, 7562 (2018).

[51] R. P. Dulal, B. R. Dahal, A. Forbes, N. Bhattarai, I. L. Pegg, and J. Philip, Weak localization and small anomalous Hall conductivity in ferromagnetic Weyl semimetal Co_2TiGe, Scientific Reports **9**, 3342 (2019).

[52] A. R. Wildes, R. C. C. Ward, M. R. Wells, J. P. Hill, and R. A. Cowley, High-resolution x-ray scattering from epitaxial thin films of Y/Nb on Al_2O_3, Journal of Physics: Condensed Matter **32**, 374006 (2020).

[53] Y. L. S. Ginley, T.P.; Wang, Topological Insulator Film Growth by Molecular Beam Epitaxy: A Review., Crystals **6**, 154 (2016).

[54] S. Takahashi and S. Maekawa, Spin current, spin accumulation and spin Hall effect, Science and Technology of Advanced Materials **9**, 014105 (2008).

[55] T. Valet and A. Fert, Theory of the perpendicular magnetoresistance in magnetic multilayers, Phys. Rev. B **48**, 7099 (1993).

[56] L. O'Brien, M. J. Erickson, D. Spivak, H. Ambaye, R. J. Goyette, V. Lauter, P. A. Crowell, and C. Leighton, Kondo physics in non-local metallic spin transport devices, Nat Commun **5** (2014).

[57] D. R. Lide, ed., *CRC Handbook of Chemistry and Physics, 84th Edition.* (CRC Press. Boca Raton, Florida, 2003).